Analysis of metal-oxide-based charge generation layers used in stacked organic light-emitting diodes

Xiangfei Qi,[1] Ning Li,[1] and Stephen R. Forrest[1,2,a)]
[1]*Department of Physics, University of Michigan, Ann Arbor, Michigan 48109, USA*
[2]*Department of Electrical Engineering and Computer Science and Department of Materials Science and Engineering, University of Michigan, Ann Arbor, Michigan 48109, USA*

(Received 28 September 2009; accepted 17 November 2009; published online 13 January 2010)

We study electron and hole injection in MoO_3 charge generation layers (CGLs) commonly used for establishing balanced injection in multilayer stacked organic light-emitting diodes (SOLEDs). A compound CGL consisting of 100-Å-thick MoO_3 and Li-doped 4,7-diphenyl-1,10-phenanthroline in a 1:1 molar ratio is demonstrated to have a high electron generation efficiency. Charge injection from the compound CGL is modeled based on a two-step process consisting of tunneling-assisted thermionic emission over an injection barrier of (1.2 ± 0.2) eV and a trap level due to oxygen vacancies at (0.06 ± 0.01) eV above the MoO_3 valence band edge. Peak external quantum efficiencies (EQEs) of $(10.5\pm0.2)\%$, $(10.1\pm0.2)\%$, $(8.6\pm0.2)\%$, and $(8.9\pm0.2)\%$ are obtained for tris-(phenylpyridine)iridium-based electrophosphorescent OLEDs with indium tin oxide (ITO) anode/CGL cathode, CGL anode/CGL cathode, CGL anode/Al cathode, and ITO anode/Al cathode contacts, respectively. Based on our analysis, a three-element green emitting electrophosphorescent SOLED is demonstrated with a peak forward-viewing EQE$=(24.3\pm1.0)\%$ and a power efficiency of (19 ± 1) lm/W. © *2010 American Institute of Physics*. [doi:10.1063/1.3275050]

I. INTRODUCTION

Due to their importance in stacked organic light-emitting diode (SOLED) and tandem organic solar cell performance,[1,2] attention has focused on developing efficient charge generation layers (CGLs) employing stable metal oxides.[3–5] To optimize such layers, an understanding of the charge generation mechanism must be developed. In past work, tunneling based on field-induced charge carrier separation at doped organic/organic heterointerfaces was used to model their performance.[6] Yet the physics of the metal-oxide-based carrier generation process has not yet been adequately explored.

We have recently reported on efficient R-G-B SOLEDs using transparent, compound CGLs consisting of MoO_3 adjacent to Li-doped 4,7-diphenyl-1,10-phenanthroline (BPhen).[7] The device yielded a peak total external quantum efficiency (EQE) and power efficiency (PE) of $\eta_{ext}=(36\pm2)\%$ and $\eta_p=(21\pm1)$ lm/W at current densities of $J=82$ μA/cm^2 and $J=17$ μA/cm^2, respectively. Both the high efficiency and white balance achieved in this SOLED indicate that efficient charge generation and injection can be obtained using MoO_3,[8] and the results may be generalized to other compound CGLs such as Mg:tris-(8-hydroxyquinoline)-aluminum(Alq_3)/WO_3 and Mg:Alq_3/V_2O_5.[9,10]

To further understand and optimize the CGL architecture, in this work we systematically study the charge generation in CGLs based on transparent metal oxides. We analyze the current density-voltage (J-V) and capacitance-voltage (C-V) characteristics of electron- and hole-only devices consisting of MoO_3 layers with varying thicknesses and over a wide range of temperature. Optimized performance of a Li:2,9-dimethyl-4,7-diphenyl-1,10-phenanthroline (BCP)/MoO_3 CGL is demonstrated by varying both the thickness of MoO_3 and the Li doping ratio in BCP. Thermally assisted tunneling from a trap level at (0.06 ± 0.01) eV above the MoO_3 valence band maximum into the adjacent organic layer is proposed to explain the temperature dependence of the J-V characteristics in both electron- and hole-only devices. The results show the importance of maintaining charge balance in each subelement to achieve high quantum efficiency.[11] Based on our analysis, we demonstrate a three-element green electrophosphorescent SOLED whose energy-level diagram is shown in Fig. 1(a), establishing charge balance and comparable efficiency for each element in the stack having a different anode/cathode combination.

This paper is organized as follows: In Sec. II, the thermionically assisted tunneling injection model is proposed, followed by experimental details in Sec. III. The results are presented in Sec. IV and are analyzed in Sec. V. We apply our results to designing and demonstrating an efficient, three-element green electrophosophorescent SOLED, also described in Sec. V. In Sec. VI, we present conclusions.

II. THEORY

We base our analysis on the hypothesis that electron injection occurs via thermionically excited electrons into traps located at energy, ϕ_t, above the MoO_3 valance band maximum, as shown in Fig. 1(b). This is followed by field-assisted tunneling through the thin depletion region of the adjacent, doped organic layer. At applied voltage, V, the electron ($J_{e,CGL}$) and hole ($J_{h,CGL}$) current densities in the CGL interface region in Fig. 1 are as follows:

a)Electronic mail: stevefor@umich.edu.

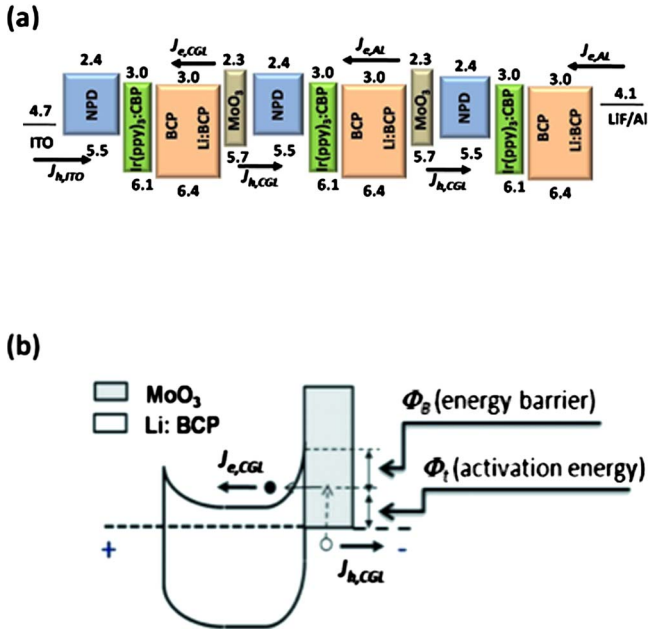

FIG. 1. (Color online) (a) Proposed energy-level diagram of a three-subelement tris-(phenylpyridine)iridium [$Ir(ppy)_3$] SOLED. The numbers indicate the highest occupied molecular orbital (HOMO) and lowest unoccupied molecular orbital (LUMO) energies relative to vacuum (in eV). The HOMO and LUMO energies of $Ir(ppy)_3$ are 5.1 and 2.6 eV, respectively. The arrows indicate the carrier injection direction, with $J_{h,\mathrm{ITO}}$, $J_{e,\mathrm{Al}}$, and $J_{e(h),\mathrm{CGL}}$ indicating electrons (holes) injected from ITO, Al, and CGL, respectively. (b) Energy level of CGL in the proposed thermally assisted tunneling model, where ϕ_t is the trap level with respect to MoO_3 valence band maximum, and ϕ_B is the tunneling barrier. Holes (open circle) and electrons (solid circle) are dissociated under the electric field, resulting in current density of $J_{h,\mathrm{CGL}}$, and $J_{e,\mathrm{CGL}}$, respectively.

$$J_{e,\mathrm{CGL}} = J_{h,\mathrm{CGL}} = qv_e N_t f P(V), \tag{1}$$

where $f = 1/1+\exp[q\phi_t/kT]$ is the Fermi–Dirac function, q is the elementary charge, k is Boltzmann's constant, T is the temperature, ϕ_t is the trap level above the MoO_3 valence band maximum, v_e is the electron thermal velocity,[12] N_t is the trap concentration, and $P(V)$ is the tunneling probability over an interface barrier of height, ϕ_B.[13] Now,

$$P(V) = \exp\left[-\frac{\alpha}{E(V)}\phi_B^{3/2}\right], \tag{2}$$

where $\alpha = 4\sqrt{2m_s^*q}/3\hbar$ for a triangular energy barrier. Here, $E(V)$ is the electric field at voltage, V, m_s^* is the electron effective mass in the organic semiconductor, and $\hbar$ is Planck's constant divided by 2π.

We note that in earlier work, Fowler–Nordheim tunneling has been used to explain the conduction characteristics of metal oxides diodes such as $Al-Al_2O_3-Au$. While a weak temperature dependence observed in that work was attributed to "compensation effects"[14] that follow an Arrhenius equation, to our knowledge no *quantitative* fit to that temperature dependence [as in Eq. (1)] has been shown.

Aside from providing efficient carrier injection, the CGL must establish charge balance in adjacent subelements in a stacked device. Charge balance can be realized by the use of blocking layers[15] or by balanced carrier injection. For a discrete OLED, charge balance is maintained by Ohmic injection of electrons and holes into the light emissive layer

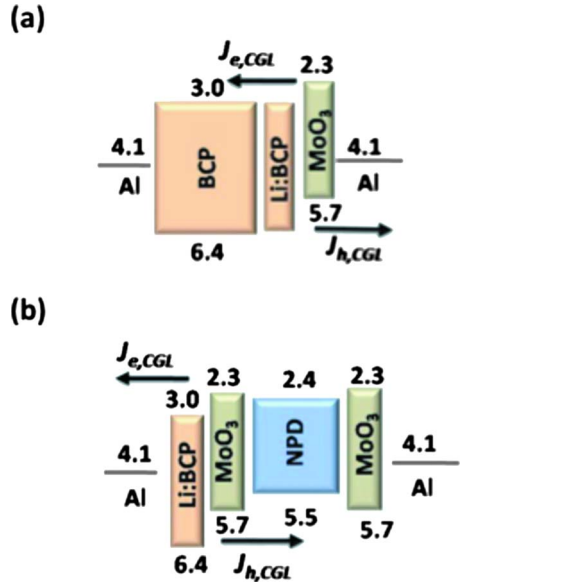

FIG. 2. (Color online) Proposed energy-level diagrams of the (a) electron-, and (b) hole-only devices.

(EML). This process is more complicated in a SOLED, considering the increased number of energy barriers to hole and electron injection that exist between counterelectrodes.

Now, the exciton generation rate at current density J is[16]

$$G(J) = \int G(x,J)dx = \frac{1}{q}\int \frac{d[J_e(x)]}{dx}dx = -\frac{1}{q}\int \frac{d[J_h(x)]}{dx}dx \equiv \frac{1}{q}J\gamma, \tag{3}$$

where $G(x,J)$ is the volume generation rate of excitons between positions x and $x+dx$ in the EML, with $x=0$ taken at the EML/electron transport layer (ETL) interface. The integration is across the entire width of the EML. The charge balance factor, γ, is the ratio of holes to electrons injected into the EML,[17] given by

$$\gamma = \frac{J_{h,A} - J_{h,C}}{J} = \frac{J_{e,C} - J_{e,A}}{J}, \tag{4}$$

where $J_{h,A}$, $J_{h,C}$, $J_{e,A}$, and $J_{e,C}$ are the hole (h) and electron (e) current densities at the anode (A) and cathode (C) sides of the EML. For high-efficiency electrophosphorescent OLEDs, the charge balance factor is near unity,[18] indicating that equal numbers of electrons and holes are simultaneously present in the recombination zone.

III. EXPERIMENTAL

Both the electron- and hole-only devices were prepared on detergent and solvent cleaned glass substrates that were immediately transferred into a vacuum chamber with a base pressure of 10^{-7} Torr after a 10 min exposure to an UV/ozone treatment.[19] For the electron-only device shown in Fig. 2(a), a 50-nm-thick Al cathode to minimize hole injection was deposited onto the glass substrate through a 1-mm-wide striped shadow mask. This was followed by the deposition of a 40-nm-thick layer of BCP and a 10-nm-thick Li-

doped layer of BCP in a 1:1 molar ratio. On this surface, a layer of MoO_3 of different thicknesses (5, 10, and 20 nm) was deposited, followed by a second 50-nm-thick Al cathode deposited through a 1-mm-wide striped shadow mask positioned perpendicular to the anode stripes. Similarly, for the hole-only device [see Fig. 2(b)], a 50-nm-thick Al electrode was deposited onto the glass substrate, followed by the deposition of a 10-nm-thick Li-doped BCP with 1:1 molar ratio and MoO_3 of varied thicknesses (0, 5, 10, and 20 nm). Then 40-nm-thick 4,4′-bis[*N*-(1-naphthyl)-*N*-phenyl-amino]-biphenyl (NPD) was deposited as a hole transport layer (HTL), followed by a 50-nm-thick MoO_3 electron blocking layer (EBL), and capped by a 50-nm thick Al cathode.

The ionization potentials and work functions used in the energy-level diagrams have been taken from the literature.[20,21] Note, however, that there remains disagreement for some of these values, with the range particularly large for MoO_3.[22] For the purposes of this work, we use a work function of 5.7 eV,[20] consistent with the values obtained for material deposited using methods similar to those employed here. For example, recent experiments[23] replacing MoO_3 with an organic thin film as an electron blocking layer provides additional support to our choice of the MoO_3 valence band energy given in Figs. 1 and 2. Finally, photoelectron spectroscopic data in our laboratory (to be reported elsewhere) obtained for the film growth methods and material compositions used here are consistent with the more shallow assignment of the valence maximum.

For characterization, samples were mounted in a cryostat where the temperature was varied from 159 to 296 K, and *J-V* characteristics were measured using a parameter analyzer (HP 4145B). The *C-V* measurements employed an impedance/gain-phase analyzer (HP 4194A), from which we infer the free carrier concentration and position of the interface barrier. The *C-V* measurements were obtained at a frequency of 200 Hz, which is sufficiently low to allow for dielectric relaxation.[24] Optical characterization of the devices employed a calibrated detector reference using standard methods described previously.[25]

IV. RESULTS

The room temperature *J-V* characteristics of the electron-only device with MoO_3 thicknesses of 50, 100, and 200 Å are shown in Fig. 3(a). For electron injection, the Al electrode on the BCP side is positively biased relative to the Al electrode on the MoO_3 side. The lack of rectification of the *J-V* characteristics indicates nearly equally efficient electron injection from the CGL and the cathode.[6] Under forward bias ($V>0$), a dependence on MoO_3 thickness is observed, with 100 Å the optimized thickness for the electron-only devices. Figure 3(b) shows the hole-only device with no MoO_3 introduced, the current densities at a given forward bias are reduced with the temperature ranging from 159 to 296 K, and a rectification ratio of $\sim 10^4$ at ± 5 V is observed at room temperature.

The *C-V* characteristics of the electron-only devices are shown in Fig. 4(a). Depletion layer widths calculated from the capacitance[26] are shown in Fig. 4(b). In Fig. 4(c), the effect of different free carrier concentrations on interface depletion width is demonstrated for CGLs with a 100-Å-thick layer of MoO_3. The concentrations of Li in BCP are varied from 1:1 to 1:10 molar ratio, corresponding to depletion widths of 24 and 85 Å, respectively. The device without Li doping shows a fully depleted region with a thickness of 110 Å.

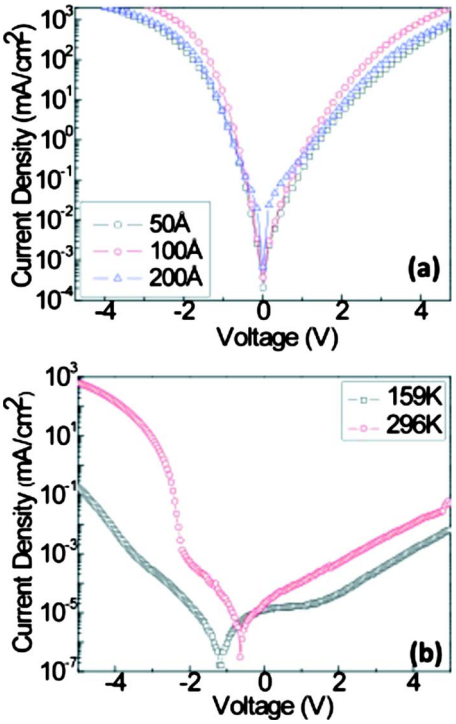

FIG. 3. (Color online) (a) Room-temperature *J-V* characteristics of the electron-only devices with MoO_3 of thickness 50 Å (square), 100 Å (circle), and 200 Å (triangle). (b) The *J-V* characteristics of the hole-only device (Al 500 Å/Li:BCP 100 Å/NPD 400 Å/MoO_3 50 Å/Al 500 Å) at 159 K (open square) and 296 K (open circle).

The current densities as functions of $1/E(V)$ for various temperatures ranging from 159 to 296 K are plotted for electron-only (Fig. 5) devices shown in Fig. 2(a). Here, the electric field is taken as the ratio of the applied voltage to the charge generation layer thickness, after subtracting the 2.7 V built-in potential. Small voltage drops at the contact/organic layer interface and across the highly Li-doped layers are neglected. In Fig. 6, the current densities J versus $1000/T$ are plotted for an electric field $E=2.0\times 10^7$ V/cm, from which we obtain the trap activation energy ϕ_t. Corresponding plots for hole-only devices are shown in Figs. 7 and 8, respectively.

V. DISCUSSIONS

A. Thermally assisted tunneling injection

The presence of MoO_3 is required for efficient charge generation, as shown by comparison of Figs. 3(a) and 3(b). Under reverse bias, both Al contacts are nearly Ohmic due to the high Li concentration in BCP, as well as due to the 50-Å-thick MoO_3 between the NPD and the Al cathode, which, in combination, enhances hole injection.[20] Under forward

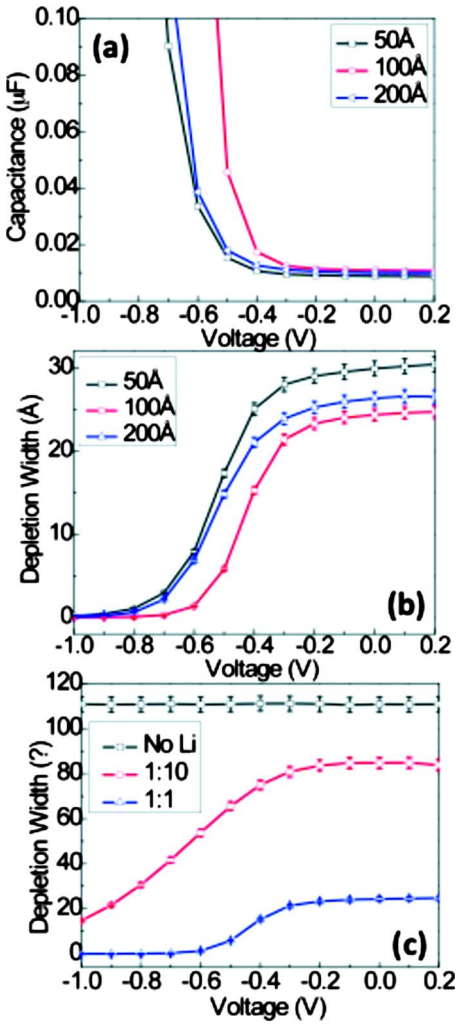

FIG. 4. (Color online) (a) The *C-V* characteristics and (b) calculated depletion widths of the electron-only devices with MoO_3 of the thickness 50 Å (square), 100 Å (circle), and 200 Å (triangle) at frequency of 200 Hz. (c) Calculated depletion widths of the electron-only devices with 100-Å-thick MoO_3 with Li: BCP in a 1:10 molar ratio (circle) and Li: BCP in a 1:1 molar ratio (triangle), and without Li doping (square).

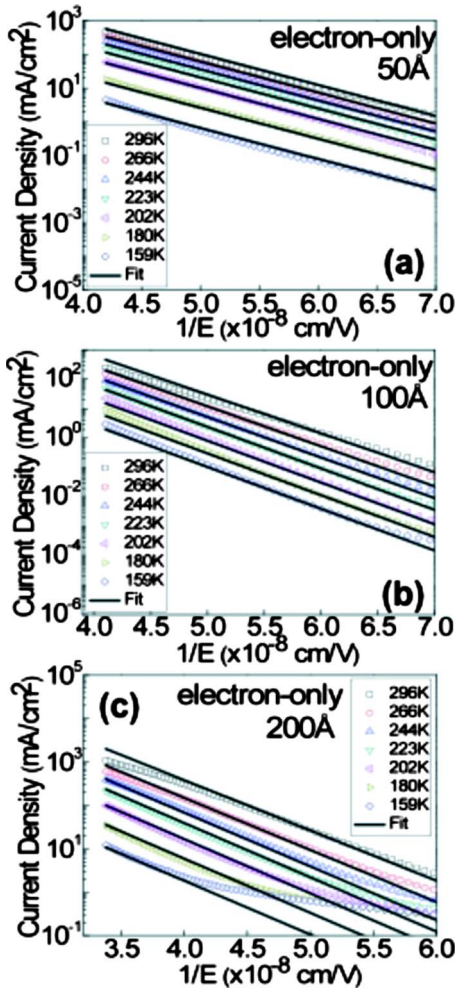

FIG. 5. (Color online) Current density (*J*) vs inverse electric field (*E*) for electron-only devices with MoO_3 thicknesses of (a) 50 Å, (b) 100 Å, and (c) 200 Å under temperatures that varied from 159 to 296 K. The solid lines are fits according to the tunneling-assisted thermionic emission model.

bias, however, both electron and hole injections are reduced at the electrodes, and the current density is a result of carrier generation from the CGL. With efficient injection and transport facilitated for both electrons and holes under both reverse and forward biases, symmetric *J-V* characteristics are observed for electron-only devices with various MoO_3 thicknesses, as shown in Fig. 3(a). Among the CGLs with varied thicknesses of MoO_3, the device with a 100-Å-thick CGL shows a high generation efficiency, with a current three to four times higher than for 50- and 200-Å-thick MoO_3 layers at >2 V under forward bias. The MoO_3 is too thin to result in complete and uniform coverage at 50 Å, hence reducing injection at this interface, while at thicknesses >100 Å, tunneling injection is significantly attenuated.

The *J-V* characteristics of the hole-only devices, not shown here, yield a similar dependence on MoO_3 thickness. Shown in Fig. 3(b) are the *J-V* characteristics of a hole-only device, with the structure Al (500 Å)/Li:BCP (100 Å)/NPD (400 Å)/MoO_3 (50 Å)/Al (500 Å). Here the 50-Å-thick MoO_3 adjacent to Al cathode acts as EBL. Inefficient carrier generation was observed under forward bias due to the absence of MoO_3 at the anode, resulting in a rectification ratio of $\sim 10^4$ at ± 5 V at room temperature. The hysteresis behavior at 159 K, shown in Fig. 3(b) where zero current occurs at -1.2 V for voltage swept from -5 to 5 V, is possibly due to

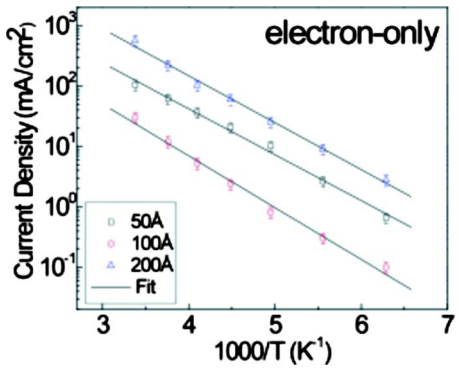

FIG. 6. (Color online) Current density (*J*) vs $1000/T$, where *T* is the temperature for electron-only devices at an applied electric field $E=2.0 \times 10^7$ V/cm, except for the device with 200-Å-thick MoO_3, $E=2.6 \times 10^7$ V/cm is used. The solid line fits yield the trap energy level, ϕ_t, listed in Table I.

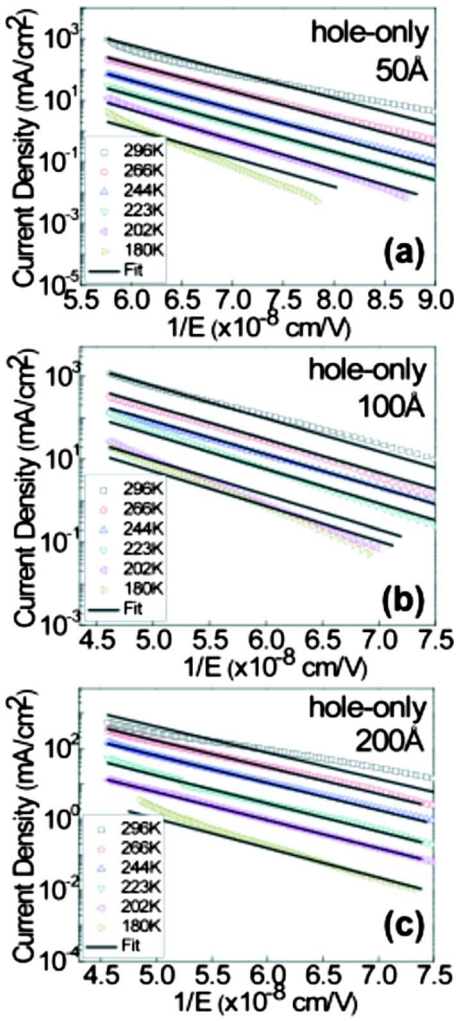

FIG. 7. (Color online) Current density (J) vs inverse electric field (E) for hole-only devices with MoO_3 thicknesses of (a) 50 Å, (b) 100 Å, and (c) 200 Å under temperatures that varied from 180 to 296 K. The solid lines are fits according to the tunneling-assisted thermionic emission model.

the electron capture and delayed re-emission at defect states in MoO_3 introduced during film deposition.[27]

To understand the thickness dependence of the charge carrier generation efficiency, C-V measurements for the electron-only devices are shown in Fig. 4(a). The depletion

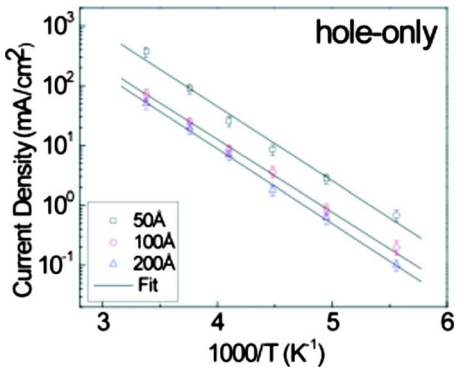

FIG. 8. (Color online) Current density (J) vs $1000/T$, where T is the temperature for hole-only devices at an applied electric field $E=1.6\times10^7$ V/cm. The solid line fits yield the trap energy level, ϕ_t, listed in Table I.

TABLE I. Tunneling barrier, ϕ_B, trap depth, ϕ_t, and trap density, N_t, of electron- and hole-only devices vs. MoO_3 thickness.

Devices		50 Å	100 Å	200 Å
Electron-only	ϕ_B(eV)	1.1 ± 0.1	1.3 ± 0.1	1.2 ± 0.1
	ϕ_t(eV)	0.07 ± 0.01	0.06 ± 0.01	0.06 ± 0.01
	$N_t(\times10^{-18}$ cm$^{-3})$	1.2 ± 0.8	12.5 ± 7.3	2.5 ± 1.4
Hole-only	ϕ_B(eV)	1.1 ± 0.1	1.0 ± 0.1	1.0 ± 0.1
	ϕ_t(eV)	0.08 ± 0.02	0.09 ± 0.02	0.09 ± 0.02
	$N_t(\times10^{-18}$ cm$^{-3})$	15.7 ± 9.2	9.9 ± 5.8	3.1 ± 1.9

widths in the doped BCP layer, are 30, 24, and 26 Å for CGLs with MoO_3 thicknesses of 50, 100, and 200 Å, respectively [Fig. 4(b)]. The relative static permittivity used to determine the carrier concentration is 3.0 for the organic layers.[28] In the case of 1:1 Li:BCP, the electron concentration in BCP is calculated to be $N_d\sim10^{19}$ cm^{-3} as inferred from the depletion width of 24 Å.[29] This is in agreement with the 1:1 molar ratio of Li:BCP doping concentration, suggesting one electron per Li atom. We conclude that both the existence of MoO_3 with the optimized thickness and the heavily doped BCP layer ensure a very thin depletion layer that allows for efficient electron injection.[30] Since the tunneling probability is an exponential function of tunneling distance, the 100-Å-thick MoO_3 sample results in the highest tunneling injection efficiency compared to the other thicknesses used.

To extract energy barrier ϕ_B, the J versus E^{-1} characteristics of the electron-only devices with various MoO_3 thicknesses are plotted in Fig. 5, where E is calculated by subtracting the built-in potential, 2.7 V, from the applied voltage. Since Li:BCP and MoO_3 are highly doped n-type and p-type semiconductor materials, respectively, the built-in potential at the Li:BCP/MoO_3 junction is determined by the difference between BCP LUMO (3.0 eV) and MoO_3 valence band maximum (5.7 eV).[20] Linear relationships in $\log(J)$ versus E^{-1} are observed for devices in the temperature range from 159 to 296 K. Energy barriers, ϕ_B, obtained from the fit of Eq. (1) to these data are listed in Table I.

To extract the trap activation energy, ϕ_t, the current densities J versus $1000/T$ for these same data are plotted in Fig. 6. The slopes of the fits (solid lines) yield $\phi_t=(0.06\pm0.01)$ eV independent of the MoO_3 thickness. The intercepts yield the value $qv_eN_t\sim10^6$ A/cm^2. Taking the electron thermal velocity of $v_e\sim10^6$ cm/s, we obtain a trap concentrations $N_t\sim10^{19}$/cm^3, as listed in Table I. The comparatively small temperature dependence of v_e ($\sim T^{1/2}$) relative to the Fermi–Dirac term allows for its omission from the model without incurring significant error.

Similar plots for hole-only devices are shown in Figs. 7 and 8. The electric field within the CGL is more complicated to estimate than for electron-only devices due to the voltage drop across the undoped NPD. Hence, we fabricated the following device: indium tin oxide (ITO) (1500 Å)/NPD (400 Å)/MoO_3 (100 Å)/Al (500 Å) to determine E. From these data, we obtain ϕ_B and ϕ_t, with the results also presented in Table I. Agreement between the energies and trap

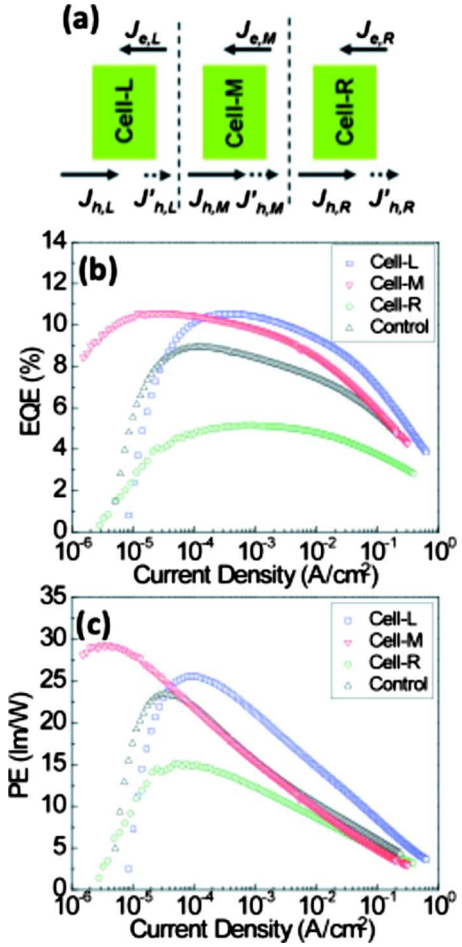

FIG. 9. (Color online) (a) Schematic of the currents that establish charge balance in a SOLED with three subelements. The directions of current densities are indicated by arrows. Parasitic leakage currents are indicated by the dashed lines. (b) EQEs and (c) PEs of cell-L (open square), cell-M (inverted triangle), cell-R (open circle), and the control device (triangle).

densities obtained for both the electron- and hole-only devices provides significant support for our model.

B. Combining multiple CGLs in SOLEDs

To determine the effects of the charge generation efficiency on the performance of a green emitting SOLED with more than two subelements, OLEDs using the CGL as either a cathode (cell-L), an anode (cell-R), or both (cell-M) were fabricated [see Fig. 9(a)], as well as the control device with an ITO anode/Al cathode combination. Detailed structures are provided in Table II. Note that for cell-R and cell-M, 20-Å-thick Al was directly deposited onto ITO to ensure band alignment at the metal/organic interface,[31] and thus to decrease the significant energy barrier that prevents electron transport from the CGL to ITO.

The EQE and PE of each device are shown in Figs. 9(b) and 9(c). The control device shows a peak forward-viewing EQE $=(8.9\pm0.2)\%$ at current density $J=0.13$ mA/cm^2, similar to previously reported Ir(ppy)$_3$-based electrophosphorescent OLEDs.[32] A peak forward-viewing EQE $=(10.5\pm0.2)\%$ is observed for cell-L at $J=0.37$ mA/cm^2 and EQE$=(10.6\pm0.2)\%$ at $J=39$ μA/cm^2 for cell-M. In contrast, cell-R shows a significantly reduced peak EQE $=(5.3\pm0.2)\%$ at a current density of $J=0.92$ mA/cm^2. The PE for cell-L, cell-M, and cell-R have maxima of (26 ± 1), (29 ± 1), and (15 ± 1) lm/W, respectively, compared to PE $=(23\pm1)$ lm/W for the control device.

TABLE II. Structure of the subcells in a three layer SOLED and the control OLED.

Devices	Layer functions	Materials	Thicknesses (Å)
Cell-L	Anode	ITO	1500
	HTL	NPD	400
	EML	Ir(ppy)$_3$:CBP	250
	ETL	BCP	500
	CGL	Li:BCP/MoO$_3$	100/100
	Cathode	Al	500
Cell-M	Anode	ITO/Al	1500/20
	CGL	Li:BCP/MoO$_3$	100/100
	HTL	NPD	400
	EML	Ir(ppy)$_3$:CBP	250
	ETL	BCP	500
	CGL	Li:BCP/MoO$_3$	100/100
	Cathode	Al	500
Cell-R	Anode	ITO/Al	1500/20
	CGL	Li:BCP/MoO$_3$	100/100
	HTL	NPD	400
	EML	Ir(ppy)$_3$:CBP	250
	ETL	BCP	400
	Cathode	LiF/Al	8/500
Control	Anode	ITO	1500
	HTL	NPD	400
	EML	Ir(ppy)$_3$:CBP	250
	ETL	BCP	400
	Cathode	LiF/Al	8/500

Since no NPD emission is observed as a function of current density for cell-L, cell-M, or cell-R, we infer that there exists no electron leakage in the three devices. The improved electron transport to the EML achieved by the CGL in cell-L and cell-M leads to enhanced EQEs. In contrast, due to enhanced hole injection from a CGL anode, cell-R shows an EQE considerably less than that of the control OLED. As suggested by Eqs. (3) and (4), to achieve high efficiency and brightness, CGLs, used in varied contact combinations must provide for charge balance in each emitting element of which the structures have to be modified according to the contact combinations for perfect charge balance. Note that optical interference effects introduced by CGLs and the thin Al layers in all three cells have been calculated based on transfer matrix simulations,[33] leading to only a small (3%) effect on the PEs, and hence cannot be the cause of the reduced EQE of cell-R.

Comparing the efficiency of the control device with those of each subelement in the stack, we obtain the following charge balance fractions for cell-L, cell-M, and cell-R [see Fig. 9(a)]:

$$\gamma_{\text{cell-L}} = \frac{J_{h,L} - J'_{h,L}}{J_{h,L}} = \frac{10.5\%}{\text{EQE}_{\max}}, \tag{5a}$$

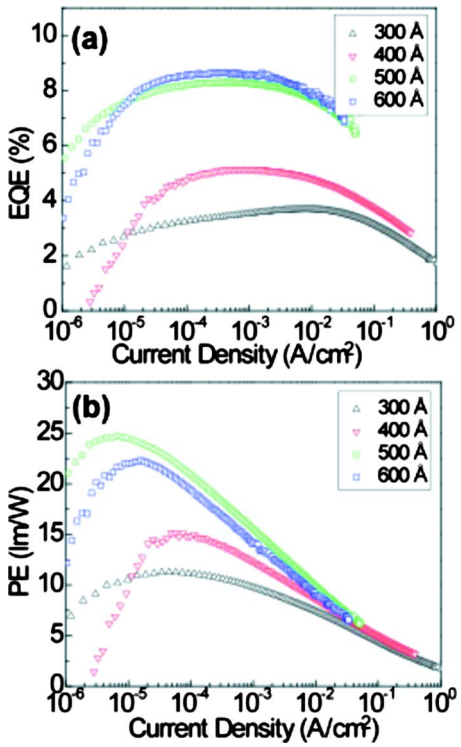

FIG. 10. (Color online) (a) EQEs and (b) PEs of cell-R with various BCP thicknesses.

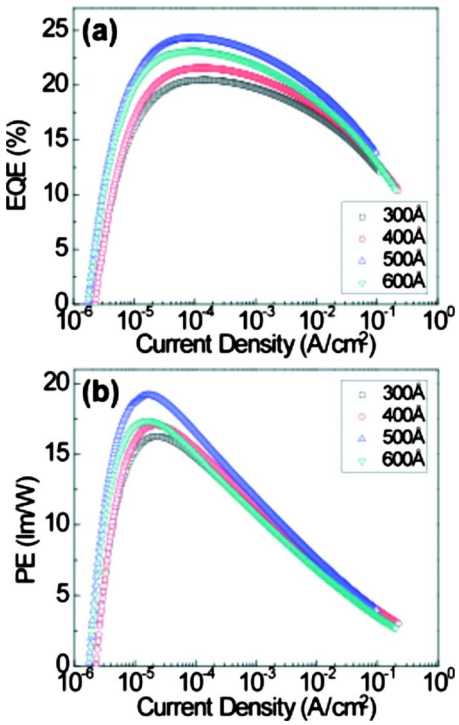

FIG. 11. (Color online) (a) EQEs and (b) PEs of G-G-G SOLEDs with various BCP thicknesses in cell-R. Note that the results are consistent with the sum of a combination of the three discrete subelements in Figs. 9 and 10.

$$\gamma_{\text{cell-M}} = \frac{J_{h,M} - J'_{h,M}}{J_{h,M}} = \frac{10.1\%}{\text{EQE}_{\max}}, \tag{5b}$$

$$\gamma_{\text{cell-R}} = \frac{J_{h,R} - J'_{h,R}}{J_{h,R}} = \frac{5.1\%}{\text{EQE}_{\max}}. \tag{5c}$$

Under charge neutrality at both electrodes, we have

$$J_{h,L} = J_{e,R} + J'_{h,R} = J_{\max} \approx 0.4 \ \text{mA/cm}^2. \tag{5d}$$

Equations (5a)–(5c) show that the charge balance factor of cell-R is approximately 50% of that achieved in cell-L and cell-M, indicating a large hole-current imbalance in cell-R. With $\text{EQE}_{\max} \sim 20\%$ achieved in Ir-based electrophosphorescence OLEDs,[18] we infer a hole leakage current of $J'_{h,R} = 0.30 \ \text{mA/cm}^2$, whose presence results in the significantly reduced EQE of that subelement.

To optimize cell-R, the hole current was controlled by using various thicknesses of BCP, ranging from 300 to 600 Å. As shown in Fig. 10, peak EQEs of $(3.7 \pm 0.2)\%$, $(5.1 \pm 0.2)\%$, $(8.3 \pm 0.2)\%$, and $(8.6 \pm 0.2)\%$ are observed for BCP thicknesses of 300, 400, 500, and 600 Å, respectively. The corresponding PEs have maximum values of (11 ± 1), (15 ± 1), (24 ± 1), and (22 ± 1) lm/W. Increased EQEs and PEs are observed for the devices with BCP thicknesses of 500 and 600 Å. Thus, by changing only the transport layer thickness (and hence its resistance), we can significantly improve cell efficiency, which supports the conclusion that charge imbalance in cell-R is the primary mechanism for efficiency loss. Of the various means of achieving charge balance, Ohmic hole and electron injection into the EML is optimal. Hence, employing charge blocking layers[15] as opposed to increasing layer resistance (as done here) provides the highest combination of PE and EQE for each element in the stack.

The EQEs and PEs of the G-G-G SOLEDs with varied BCP thicknesses in cell-R, from 400 to 600 Å, are shown in Figs. 11(a) and 11(b), respectively. Devices with 300-, 400-, 500-, and 600-Å-thick BCP exhibit forward-viewing EQEs peaking at $(20.5 \pm 1.0)\%$, $(21.6 \pm 1.0)\%$, $(24.3 \pm 1.0)\%$, and $(23.1 \pm 1.0)\%$, respectively, at a current density of $J = 1.4 \times 10^{-4}$ A/cm^2. The optimized G-G-G SOLED, with 500-Å-thick BCP in cell-R, shows a peak forward-viewing PE $= (19 \pm 1)$ lm/W at the current density of $J = 1.7 \times 10^{-5}$ A/cm^2, which rolls off to (12 ± 1) lm/W at 1000 cd/m^2 corresponding to $J = 1.2 \times 10^{-3}$ A/cm^2. The EQEs of the G-G-G SOLEDs are approximately the sum of the EQEs of the three individual OLEDs over a wide range of current densities, indicating that the losses at the transparent CGL are minimal.

Liao *et al.*[34] reported a similar Ir(ppy)$_3$-based G-G-G OLED where Li:tris(8-hydroxyquinoline)aluminum/$FeCl_3$:4,4′-bis-(1-naphthyl-*N*-phenylamino)-biphenyl was used as the CGL. Comparison of our device performance with that of Liao *et al.*, however, is difficult due to their use of cd/A for efficiency determination and the assumption that the SOLED is a pure Lambertian source (which is not accurate for devices that exhibit pronounced microcavity effects, as in this case). Nevertheless, it is reasonable to assume comparable efficiencies in both devices given that each stacked subelement is not expected to have an EQE $> 8-9\%$, as widely reported for discrete Ir(ppy)$_3$-based OLEDs.

VI. CONCLUSIONS

We have modeled carrier generation from doped organic/metal-oxide interfaces in SOLEDs based on electron injection via thermally assisted tunneling through a (1.2 ± 0.2) eV barrier and an oxygen vacancy-induce trap level at (0.06 ± 0.01) eV above the metal oxide (in this case, MoO_3) valence band maximum. Based on our model, we optimize a stacked green electrophosphorescent OLED with three subelements (G-G-G SOLED). The highest efficiency from all three elements in the stack is obtained when both carrier injection from the CGLs and the counterelectrodes are all in balance. This requires different injection electrode combinations for each element, i.e., ITO anode/CGL cathode for the bottom (anode facing) element, CGL anode/CGL cathode for the central element, and CGL anode/Al cathode for the top (cathode facing) element. Charge balance was achieved by modifying the thickness of the carrier transport layer, although the use of charge blocking layers to achieve balance in the subelement emission layer should lead to higher PEs than obtained here.

ACKNOWLEDGMENTS

The authors thank the Air Force Office of Scientific Research and Universal Display Corp. for partial financial support of this work.

[1]C. W. Law, K. M. Lau, M. K. Fung, M. Y. Chan, F. L. Wong, C. S. Lee, and S. T. Lee, Appl. Phys. Lett. **89**, 133511 (2006).
[2]J. Drechsel, B. Mannig, D. Gebeyehu, M. Pfeiffer, K. Leo, and H. Hoppe, Org. Electron. **5**, 175 (2004).
[3]Z. Shen, P. E. Burrows, V. Bulovic, S. R. Forrest, and E. Mark Thompson, Science **276**, 2009 (1997).
[4]T. Matsumoto, T. Nakada, J. Endo, K. Mori, N. Kawamura, A. Yokoi, and J. Kido, SID Int. Symp. Digest Tech. Papers **34**, 979 (2003).
[5]H. Kanno, N. C. Giebink, Y. Sun, and S. R. Forrest, Appl. Phys. Lett. **89**, 023503 (2006).
[6]M. Kröger, S. Hamwi, J. Meyer, T. Dobbertin, T. Riedl, W. Kowalsky, and H. H. Johannes, Phys. Rev. B **75**, 235321 (2007).
[7]X. Qi, M. Slootsky, and S. R. Forrest, Appl. Phys. Lett. **93**, 193306 (2008).
[8]H. Kanno, R. J. Holmes, Y. Sun, S. Kena-Cohen, and S. R. Forrest, Adv. Mater. (Weinheim. Ger.) **18**, 339 (2006).
[9]C. Chang, S. Hwang, C. C. Chen, and J. Chen, Jpn. J. Appl. Phys., Part 1 **43**, 6418 (2004).
[10]T. Tsutsui and M. Terai, Appl. Phys. Lett. **84**, 440 (2004).
[11]B. Krummacher, M. K. Mathai, V. Choong, S. A. Choulis, F. So, and A. Winnacker, Org. Electron. **7**, 313 (2006).
[12]S. Fleischer and P. T. Lai, J. Appl. Phys. **72**, 5711 (1992).
[13]D. M. Sathaiya and S. Karmalkar, J. Appl. Phys. **99**, 093701 (2006).
[14]T. W. Hickmott, J. Appl. Phys. **97**, 104505 (2005).
[15]C. Adachi, M. A. Baldo, S. R. Forrest, S. Lamansky, M. Thompson, and R. C. Kwong, Appl. Phys. Lett. **78**, 1622 (2001).
[16]N. C. Giebink and S. R. Forrest, Phys. Rev. B **77**, 235215 (2008).
[17]B. Ruhstaller, S. A. Carter, S. Barth, H. Riel, W. Reiss, and J. C. Scott, J. Appl. Phys. **89**, 4575 (2001).
[18]C. Adachi, M. A. Baldo, M. E. Thompson, and S. R. Forrest, J. Appl. Phys. **90**, 5048 (2001).
[19]K. Sugiyama, H. Ishii, and Y. Ouchi, J. Appl. Phys. **87**, 295 (2000).
[20]T. Matsushima, G. Jin, and H. Murata, J. Appl. Phys. **104**, 054501 (2008).
[21]T. Hori, T. Shibata, V. Kittichungchit, H. Moritou, J. Sakai, H. Kubo, A. Fujii, and M. Ozaki, Thin Solid Films (in press).
[22]M. Kroger, S. Hamwi, J. Meyer, T. Riedl, W. Kowalsky, and A. Kahn, Appl. Phys. Lett. **95**, 123301 (2009).
[23]N. Li, B. E. Lassiter, R. R. Lunt, G. Wei, and S. R. Forrest, Appl. Phys. Lett. **94**, 023307 (2009).
[24]J. Drechsel, M. Pfeiffer, X. Zhou, A. Nollau, and K. Leo, Synth. Met. **127**, 201 (2002).
[25]S. R. Forrest, D. D. C. Bradley, and M. E. Thompson, Adv. Mater. (Weinheim, Ger.) **15**, 1043 (2003).
[26]R. S. Muller and T. I. Kamins, *Device Electronics for Integrated Circuits* (Wiley, New York, 2002).
[27]F. Lindner, K. Walzer, and K. Leo, Appl. Phys. Lett. **93**, 233305 (2008).
[28]K. Nakamura, T. Hata, A. Yoshizawa, K. Obata, H. Endo, and K. Kudo, Appl. Phys. Lett. **89**, 103525 (2006).
[29]B. L. Anderson and R. L. Anderson, *Fundamentals of Semiconductor Devices* (McGraw-Hill, New York, 2004).
[30]T. Matsuo, T. Suzuki, Y. Yokoi, and S. Ikehata, J. Phys. Chem. Solids **65**, 619 (2004).
[31]M. G. Helander, Z. B. Wang, J. Qiu, and Z. H. Lu, Appl. Phys. Lett. **93**, 193310 (2008).
[32]M. A. Baldo, S. Lamansky, P. E. Burrows, M. E. Thompson, and S. R. Forrest, Appl. Phys. Lett. **75**, 4 (1999).
[33]H. Benisty, R. Stanley, and M. Mayer, J. Opt. Soc. Am. A Opt. Image Sci. Vis. **15**, 1192 (1998).
[34]L. S. Liao, K. P. Klubek, and C. W. Tang, Appl. Phys. Lett. **84**, 167 (2004).